ATR inhibition potentiates the radiation induced inflammatory tumor microenvironment

Magnus T. Dillon, Katharina F. Bergerhoff, Malin Pedersen, Harriet Whittock, Eva Crespo-Rodriguez, Emmanuel C. Patin E, Alex Pearson, Henry G. Smith, James T. E. Paget, Radhika R. Patel, Shane Foo, Galabina Bozhanova, Chanthirika Ragulan, Elisa Fontana, Krisha Desai, Anna C. Wilkins, Anguraj Sadanandam, Alan Melcher, Martin McLaughlin†, Kevin J. Harrington†

The Institute of Cancer Research, London, UK

Magnus.dillon@icr.ac.uk

†Joint senior authors

Keywords: DDR, radiosensitization, ATR inhibition, cell cycle checkpoint, mitotic catastrophe

Running Title: ATRi Plus RT Create an Inflammatory Tumor Microenvironment

Acknowledgments

This study was supported by Cancer Research United Kingdom (program grant C7224/A13407), RM/ICR NIHR Biomedical Research Centre, Rosetrees Trust (M.T. Dillon, K.J. Harrington, grant numbers M48 and M444) and Anthony Long Charitable Trust (K.J. Harrington). M.T. Dillon is a Cancer Research United Kingdom Clinical Research Fellow. We would like to thank AstraZeneca for supplying AZD6738.

Disclosure of Potential Conflict of Interest

The Institute of Cancer Research and Royal Marsden have received funding for a phase I study of AZD6738, which is partially funded by AstraZeneca.

Abstract

Purpose: ATR inhibitors (ATRi) are in early phase clinical trials and have been shown to sensitise to chemotherapy and radiotherapy preclinically. Limited data have been published about the effect of these drugs on the tumor microenvironment.

Experimental Design: We used an immunocompetent mouse model of HPV-driven malignancies to investigate the ATR inhibitor AZD6738 in combination with fractionated radiation (RT). Gene expression analysis and flow cytometry were performed post-therapy.

Results: Significant radiosensitization to RT by ATRi was observed alongside a marked increase in immune cell infiltration. We identified increased numbers of CD3+ and NK cells but most of this infiltrate was composed of myeloid cells. ATRi plus radiation produced a gene expression signature matching a type I/II interferon response with upregulation of genes playing a role in nucleic acid sensing. Increased MHC I levels were observed on tumor cells, with transcript-level data indicating increased antigen processing and presentation within the tumor. Significant modulation of cytokine gene expression (particularly CCL2, CCL5 and CXCL10) was found *in vivo*, with *in vitro* data indicating CCL3, CCL5 and CXCL10 are produced from tumor cells after ATRi + RT.

Conclusions: We show that DNA damage by ATRi and RT leads to an interferon response through activation of nucleic acid sensing pathways. This triggers increased antigen presentation and innate immune cell infiltration. Further understanding of the effect of this combination on the immune response may allow modulation of these effects to maximise tumor control through anti-tumor immunity.

Statement of Translational Relevance

AZD6738 is currently under investigation in clinical trials in combination with radiotherapy (NCT02223923). Substantial preclinical data exist on the radiation potentiating effects of drugs inhibiting components of the DNA damage response. Given the increased understanding of the pivotal role of the immune system in cancer control, it is critical to understand the effect radiosensitizer compounds have on the tumor microenvironment, specifically their impact on the immune system and its responses. AZD6738 boosts the immunogenic effect of radiation, enhancing tumor-derived cytokine production, antigen presentation and infiltration of myeloid lineage immune populations. Both inflammatory and immunosuppressive cells are increased after the combination treatment. The modulation of these responses to maximise anti-tumor immunity and effect on adaptive responses will be the subject of future study.

Introduction

In recent years, we have begun to understand that the effects of anti-cancer therapies cannot be considered purely from the narrow perspective of their ability to kill cancer cells effectively. Instead, their effects on the tumor microenvironment are increasingly recognised as playing a major role in the success or failure of treatment. An appreciation of the importance of the immune system to cancer surveillance, development and response to treatment has highlighted the effect that radiation has on the microenvironment, and has served as a driver of research into combinations of radiation and immune-targeted therapies (1). At the same time, increasing recognition of the effect of the vasculature and stroma on tumor control and normal tissue side-effects of radiotherapy has highlighted potential new targets for intervention (2).

Radiation has positive and negative effects on the tumor microenvironment. Radiation increases antigen presentation and T-cell priming, and can stimulate systemic (abscopal) anti-tumor responses, particularly when co-administered with immune checkpoint blockade (3). On the other hand, it can stimulate suppressive cells such as myeloid-derived suppressor cells (MDSCs) and tumor-associated macrophages (TAMs), which have been associated with tumor angiogenesis and invasion (4). Links between the DNA damage response (DDR) and both autoimmunity and anti-cancer immunity are increasingly being described. The STING pathway, activated by cytosolic DNA, stimulates type I interferon production, leading to immune responses (5). Defective DDR, S-phase DNA damage and micronucleus formation can trigger interferon production and alter the expression/function of cell surface immunomodulatory molecules (6-8). Targeted anti-cancer therapies can also exert diverse effects on the immune microenvironment (9). Few data have been reported on the microenvironmental effects of radiation in combination with radiosensitizing agents, such as DDR inhibitors. Understanding these effects may provide opportunities for further therapeutic benefit, especially in terms of immunotherapy strategies.

Here, we show that the ATR inhibitor, AZD6738, alone and in combination with a clinically relevant fractionation schedule of radiotherapy modulates the immune tumor microenvironment. To our knowledge, this is the first comprehensive profiling of the immune tumor microenvironment in the context of targeted radiosensitization.

Materials and Methods

Animals and cell lines

All experiments were approved by the Institutional Review Board and complied with National Cancer Research Institute guidelines (10). TC-1 cells – a modified mouse lung epithelial cell line transformed with HPV-16 E6 and E7 and oncogenic HRAS - were a kind gift from Prof. Tzyy-Choou Wu, Johns Hopkins University, Baltimore, USA (11) and Prof. Eric Deutsch, Institut Gustave Roussy, Villejuif, France. Two million cells were injected subcutaneously into the right flank of female C57Bl/6 mice; treatments were started 7-8 days later, at which point tumors were 50–100 mm^3. The experimental endpoint for growth delay experiments was a tumor diameter of 15 mm or greater.

Drugs

AZD6738 was provided by AstraZeneca and was dissolved in 10% DMSO, 40% propylene glycol, 50% water and administered by oral gavage, 2 hours before irradiation. For hypoxia studies, pimonidazole (Hypoxyprobe, HPI, Burlington, USA) 60 mg/kg was injected intraperitoneally 1 hour prior to tissue collection.

Irradiation

Animals were irradiated under anaesthesia with hypnorm (Fentanyl/fluanisone, Vetapharma, Leeds, UK) and Midazolam (Roche) given intraperitoneally. Irradiation was performed using an AGO 250 kV X-ray machine at a dose rate of 1.62 Gy/min (AGO, Reading, UK). Animals were irradiated in the prone position positioned under lead shielding with a 16 mm diameter aperture aligned over the tumor. Radiation dose was measured using a Farmer chamber and Unidos-E dosemeter (both PTW, Freiburg, Germany).

Immunophenotyping

Viability dye: eBioscience fixable viability dye eFluor 780 (65-0865-14). Antibodies: conjugated antibodies were obtained from BioLegend (San Diego, USA) unless otherwise stated. Antibodies used are shown in supplementary table 1. Tumors were harvested and kept on ice, then blotted dry and weighed before mechanical dissociation with scissors and enzymatic digestion for 30 minutes at 37 ºC with (per sample) 40 μL 0.25% trypsin, 20 μL collagenase (Sigma C1639 25 mg/mL in PBS), 2 μL dispase (200 mg/mL) and 10 μL DNAse (20 mg/mL), before passing through a 70 μm cell strainer and rinsing with RPMI supplemented with 10% FCS and 5 mM EDTA. Samples were resuspended in PBS with 5 % FCS, blocked with anti-CD16/32 antibody (BioLegend 101319) for 10 mins on ice then stained immediately on ice in a staining volume of 40 μL, diluting antibodies at the dilutions given in supplementary table 1 in PBS with 5% FCS for 30 minutes before washing twice.

For intracellular epitopes, samples were fixed and permeabilized after staining for extracellular epitopes, using the FoxP3/Transcription factor Fixation/Permeabilization kit (eBioscience 00-5521-00, Thermo Fisher, Waltham, USA) in accordance with the manufacturer's protocol. Subsequent staining was performed using the permeabilization buffer from this kit. After fixation, samples were washed twice and fixed using 1% formaldehyde in PBS before acquisition on a BD LSRII flow cytometer (BD Biosciences, Oxford, UK). Photomultiplier tube voltages were set using fully stained samples, and compensation was performed using single-stained UltraComp eBeads (eBioscience). Gating was performed using 'fluorescence minus one' controls and a limited number of isotype controls were used (supplementary table 1). The sample was divided equally into staining panels and each sample was acquired entirely. Data were analysed using FlowJo software (FlowJo, Ashland, USA); counts were normalised to tumor weight and corrected for the number of panels into which the sample was divided.

RNA analysis

Tumor samples were harvested from animals and stored in RNALater (AM7020, Thermo Fisher) at -20 ºC prior to RNA extraction. Samples were processed by homogenization using a Precellys24 homogenizer (Bertin Technologies, Montigny, France) and RNA extraction performed using RNEasy kit (74104, Qiagen, Germantown, USA) as per manufacturer's protocol. Paired CD45-negative and CD45-positive samples were generated by disaggregation and staining using CD45 30-F11 as for immunophenotyping. Sorting was performed using a FACS Aria III. Samples were kept on ice at all times other than enzymatic digestion, sort was performed under chilled conditions. RNA extraction on sorted cell pellets was by RNEasy kit. Extracted RNA was quantified using a NanoDrop spectrophotometer (Thermo Fisher) and quality assessed on a BioAnalyzer 2100 (Agilent, Santa Clara, USA). Samples were stored at -80 ºC before further analysis. 100 ng RNA was used for the analysis using the nCounter PanCancer Immune Profiling Panel (XT-CSO-MIP1-12, NanoString Technologies, Seattle, USA). Data analysis was performed using the nSolver advanced analysis software (NanoString Technologies). PTPRC (CD45) transcript counts in sorted samples post-normalisation ranged from 20-129 in CD45-negative and 9234-11298 for CD45-positive samples. As a precaution, minor CD45-positive contamination of treated CD45-negative samples (0.9-0.3%) was corrected for by subtraction of the corresponding % of transcripts from paired CD45-positive samples calculated based on PTPRC transcript counts. This was to avoid false positive changes associated with isolated high transcript genes. Differential expression was compared between two conditions, p-values were

adjusted using the Benjamini-Yekutieli false discovery rate; genes with adjusted p-values < 0.05 are displayed. Functional annotations were based on gene ontology terms.

Immunohistochemistry

Immunohistochemistry was performed at the Breast Cancer Now core histopathology facility, using the following primary antibodies. Dako Flex Envision (K8002) was used as the secondary reagent: p^{S345}Chk1, Thermo Fisher PA5-34625; CD3, Dianova clone SZ31, DIA-310; CD45R, Abcam ab64100; Pimonidazole, hypoxyprobe, MAb1; Carbonic Anhydrase IX: Abcam ab15086; Smooth muscle actin, Dako clone 1A4, M0851.

Western blot

Snap frozen tumour samples were lysed in RIPA buffer using a Precellys 24 homogenizer (Bertin Technologies). All lysates were quantified by BCA assay (Thermo Fisher) prior to SDS-PAGE and western blotting. The following antibodies were used: GAPDH 14C10, MDA5 D74E4 and cGAS D3O8O (Cell Signaling). Secondary was IRDye 800CW Goat anti-Rabbit IgG H + L and imaged using a LI-COR Odyssey CLx (LI-COR Biosciences).

Statistical analyses

Statistical analysis was performed using Prism 7 (GraphPad Software, San Diego, USA). For tumor growth delay, means of radiation and radiation + ATRi groups were compared using Student's unpaired t-test. Flow cytometry cell counts, mRNA count and proportions and fluorescence data were compared using one-way ANOVA with Tukey's multiple comparisons test. An asterisk indicates $p \leq 0.05$. Where multiple asterisks are used, ** indicates $p \leq 0.01$, *** indicates $p \leq 0.001$ and **** indicates $p \leq 0.0001$.

Results

ATRi and ATRi-RT modulate the immune microenvironment

Two participants in the dose-escalation study of AZD6738 monotherapy (12) had tumor volume reductions. We noted that this was associated with an inflammatory infiltrate in one of the participants, and hypothesised that AZD6738 may have a modulating effect on the immune tumor microenvironment. We sought to investigate how AZD6738 may modulate radiation induced changes to the tumor microenvironment (TME).

TC-1 is an immunocompetent model of HPV-driven malignancies. This model was chosen as it has previously been used for examining immune responses to radiotherapy combinations, and it was moderately sensitive to combination therapy, allowing sufficient tumor for analysis at the time point chosen. Mice bearing subcutaneous TC-1 tumors were treated 8 days after implantation, at which point tumors were 50 – 100 mm^3. Mice were dosed with vehicle or AZD6738 (75 mg/kg daily), starting 2 hours before the first dose of radiation, with the last dose given on day 5. Irradiation was given daily, 2 hours after drug or vehicle dosing, at 2 Gy per fraction for 4 days. ATR inhibition sensitised this model to radiation, with significantly greater tumor growth delay (Fig. 1A) and a significant increase in survival to humane endpoint (Supp. Fig. 1A).

Initial profiling of the TME was carried out 5 days after irradiation on formalin-fixed tissue. This was focused on broad markers investigating vessel density, hypoxia, fibroblasts, CD3+ (T) and CD45R/B220+ (B) cells. Because hypoxia is an important determinant of radiosensitivity, we wanted to examine whether the radiosensitization by AZD6738 was due to modulation of perfusion or hypoxia. Microenvironmental markers of hypoxia (pimonidazole, CAIX) and fibroblasts (αSMA) did not differ significantly between treatment groups (Supp. Fig 2A-C). Vessel density after 4 x 2 Gy measured by CD31 had significantly reduced compared with control. When AZD6738 was added to radiation this reduction was reversed (Supp. Fig 2D). We did observe increased numbers of T-cells (Fig. 1B) and B cells (Fig. 1C) after combination treatment with radiation and AZD6738. Given these findings, further work focussed in detail on the effect of ATRi plus radiation (ATRi-RT) on the immune tumor microenvironment.

ATRi-RT modulates multiple immune-related genes

NanoString-based expression profiling of TC-1 tumors was carried out to comprehensively profile gene expression changes 5 days after the end of radiation. This time point was selected initially to focus more on infiltrating immune population markers post-DNA damage. This revealed changes in expression in multiple categories of genes due to radiation or AZD6738 alone, with the addition of AZD6738 potentiating radiation-induced changes (Fig. 2A). This was particularly pronounced in the gene ontology groups CD molecules, apoptosis, adaptive, antigen processing and MHC. Numbers of genes with significant differential expression are shown in Fig. 2B. Strikingly, we found evidence of an interferon response, with large changes in expression of a number of interferon-stimulated genes (Fig. 2C (13), supp. fig. 3, 4). Numerically, the combination of ATRi and radiation caused the largest number of changes and greatest degree of change in gene expression.

These gene expression changes suggest infiltration and activation of innate and adaptive immune cells, which was maximal after combined ATRi-RT treatment.

ATRi-RT increases lymphocyte infiltration

Flow cytometry was used to validate specific intratumoral cell population data identified by gene expression analysis presented in Figure 2. A more focused analysis was also undertaken in the draining lymph nodes (DLN). The general lymphoid gating strategy for FACS analysis is shown in supplementary Fig. 5 and 6.

Greater numbers of total CD3+ cells over control were demonstrated after treatment with ATRi, radiation, and maximal levels were seen with combination therapy (Fig. 3A, this observation was maintained when analysed for the total number of cells, supp. Fig. 7). There were also significantly increased numbers of CD4+ FOXP3+ T_{regs} and NK cells. There was a non-significant trend towards increase in CD8+ cells observed with combination therapy (Fig. 3A), with a higher proportion of CD8+ granzyme B+ as well as CD8+ Ki67+ cells observed with combination therapy (Fig. 3B). This correlated with transcript-level data observed, where *Cd8a*, granzyme B (*Gzmb*) and perforin (*Prf1*) were highest in the combination group (Fig 3C).

Analysis of markers of activation and proliferation showed a significantly increased proportion of proliferating T_{regs} with the combination treatment (Fig. 3B). These results confirmed the transcriptional analysis which showed increased T-cell-associated and *Foxp3* transcripts in tumors (Fig. 3C). The draining lymph nodes also contained an increased proportion of proliferating Ki67+ T_{regs} as a function of total T_{regs} (Fig. 3D).

To further define infiltrating lymphocytes, flow cytometry was performed on T-cell subsets with a selection of markers (Fig. 3E). While not statistically significant, a consistent trend was observed for increased expression of LAG3, TIM3, ICOS and CTLA4 on CD4+ effector cells in the ATRi-RT combination group. No significant changes in fluorescence were found in T_{regs} or CD8+ T cells (data not shown). Similar but more statistically significant changes were observed at the transcript level. *Havcr2* (TIM3), *Tigit*, *Icos* and *Eomes* were upregulated in ATRi-RT compared with control or either monotherapy (Supp. fig. 8A). Further mRNA analysis showed increased numbers of transcripts associated with a T_h1 response, including *Il12rb2*, *Ctla4* and *Stat4* (Supp. fig. 8B) between control and RT, control and ATRi-RT. When transcriptional analysis was performed on sorted CD45-postive tumor-infiltrating cells alone, there was a significant increase in *Gzmb* transcripts (Fig. 3F). Taken together, these data suggest increased T_{reg} proliferation as well as evidence of CD4 effector cell activation or exhaustion with combination treatment.

ATRi-RT causes an increase in myeloid cell infiltration

Further validation of gene expression data identified that AZD6738 and radiation induced substantial infiltration of myeloid innate immune cells (Fig 4A, supp. fig. 7B). The general myeloid gating strategy for FACS analysis is shown in supplementary Fig. 6. A significant increase was seen in tumor-infiltrating dendritic cells (DCs), macrophages (Mac), and a CD11b+Gr1+ population (Fig. 4A)(14). This increase was clear but not statistically significant compared to controls for both monotherapies, but highest and statistically significant for ATRi in combination with radiation. In absolute numbers, the cumulative infiltration of these three populations was approximately three times the total number of CD3+ cells in the combination group (Fig 3A; Fig 4A).

Flow cytometry was used to determine if ATRi-RT altered specific subpopulations of DCs, macrophages or CD11b+Gr1+ cells. Based on CD206 staining, we did not detect any change in the proportions of M2-like macrophages (Fig 4B). Ly6C, a monocytic marker, showed that there was no clear shift in the monocytic CD11b+Gr1+ cell population with combination treatment vs control (Fig. 4C). On the other hand, granulocytic marker Ly6G staining showed that the numbers of granulocytic CD11b+Gr1+ cells were lower (supp. fig. 6). Two subsets of DC, classical (cDC) and plasmacytoid (pDC), were investigated because pDC have toll-like receptors 7 and 9, which sense RNA and DNA, respectively. We hypothesised that the increased DNA damage with ATR inhibition may activate these pattern recognition receptors. Tumor-associated pDC may increase tumor antigen presentation or may be tolerogenic (15). B220 has been described as a marker for pDC in CD11c+ DC (15).

No difference was found in proportions of pDC and cDC, using flow cytometric analysis of CD11c and B220 staining, with cDC making up the majority of DC within the tumor, and numbers of both increasing with ATRi-RT treatment (Fig. 4D). Although ATRi-RT increases both the numbers of DCs and TAMs, it does not alter the DC subsets investigated, or the polarity of TAMs.

We noted an increase in both PD-1 and PD-L1 mRNA with ATRi and ATRi-RT therapy (Supp. fig. 8C), which confirmed flow cytometry analysis, finding that the predominant increase in PD-L1 signal was from CD45+ CD3- cells, with a relatively minor contribution from tumor cells (Fig. 4E). Transcriptional analysis of sorted tumor-infiltrating immune cells and CD45-negative cells, a surrogate for tumor cells, showed a significant increase in *Cd274* (PD-L1) transcripts in both populations (Fig. 4F). Previous data have shown that tumor-infiltrating MDSC and macrophages are PD-L1+ (16, 17), and our observations have confirmed this, with increasing PD-L1-positivity after treatment with ATRi, radiation, and the combination (Fig. 4E).

Using pan-cytokeratin as a marker for tumor cells, we observed a significant increase in MHC-I expression with all conditions compared with control (Fig. 4F). Pan-cytokeratin is generally expressed on tumor cells, but may not be specific to these. mRNA expression data confirmed the increase in H2 complex molecules on CD45-negative cells, as well as a number of other components involved in antigen processing and presentation on both CD45-positive and –negative cells. These include H2 class I on tumor cells, class II on immune cells, and other genes involved in the antigen presentation processes (Fig. 4H).

ATRi and radiation drives immune cell infiltration through tumor cell-intrinsic cytokine release

ATRi and radiation clearly drive immune cell infiltration, particularly of the myeloid compartment, in response to therapy. The process driving this infiltration was, however, not clear. To investigate the potential trigger for immune cell infiltrates seen after ATRi -RT, differential expression for cytokine and cytokine receptor mRNAs was analysed (Fig. 5A). In all cases statistically significant changes were observed at the transcript level for ATRi-RT. The greatest changes after the combination of ATRi-RT were in *Ccl5*, *Il1r2* (IL-1 receptor 2), *Il2rb*, *Il2ra*, *Ccr2*, *Ccr7* and *Cxcl9*. In addition, we performed mRNA analysis on tumor cell populations sorted for CD45, which confirmed the large increases seen in *Ccl2, Ccl5* and *Cxcl10* were predominantly from non-immune cells (Fig. 9B). These data were compared with protein expression by cytokine array (Fig. 5C). Clear correlation between increased transcript levels and increased protein expression was observed for CCL2, CCL5 and

CXCL10 in response to ATRi-RT. No differences were seen at this time point in interferon mRNA transcripts (data not shown).

Many proteins can bind dsDNA triggering an immune response, forming an innate immune recognition system for dsDNA viruses. There has been significant recent interest in the ability of cGAS-STING to trigger inflammation through recognition of cytoplasmic host dsDNA (8, 18). We checked mRNA transcript results for TLRs or potential intracellular dsDNA binding proteins which may share functional similarity to STING, as well as cGAS and STING/*Tmem173* themselves.

We observed an increase in cGAS by western blot in tumors treated with ATRi-RT, as well as an increase in the interferon-stimulated gene product IFIH1 (MDA-5) (Fig. 5D). Analysis of gene expression data in the TC-1 tumors found statistically significant increases at the transcript level were present for *Tlr1,6,7,8* and *Tlr9,* with the largest change in *Tlr9* (Fig 5E). In keeping with a role for pattern recognition receptors, we also observed an increase in *Irf7* and *8* with combination therapy (Fig. 5F). increases in pattern recognition receptors for cytoplasmic nucleic acids (19): *Ddx58*/RIG-I, and *Ifih1*/MDA5, both RNA sensors and *Zbp1*/DAI (20) and *Ddx60* (21), which sense DNA. There was no change in STING (*Tmem173*) expression (Fig. 5G). When we performed the analysis on separated immune and tumor cells, we found that treatment induced significant increases in transcript levels in the non-immune cells within the tumor (Fig. 5H). In all cases, as was observed for *in vitro* cytokine release, ATRi-RT led to the highest increase in transcript levels.

CCL2, CCL5, CXCL10 and CXCL9 increases indicate that ATRi, RT and combination treatments induce pro-inflammatory responses. There was disparity between the clear significance observed at the transcript level vs protein expression. This was attributed to the 5-day post-treatment time point originally selected for gene expression analysis to favour assessment of infiltrating immune populations. Additionally, both transcript and protein assessment was not tumor-specific. To bring clarity on both these points, cytokine release from 2 human head and neck squamous cell carcinoma cell lines *in vitro* was measured in response to ATRi, radiation, or in combination at 72 h post treatment (Fig. 5I, J). We observed maximal increase in CXCL10 and CCL3 secretion with the combination treatment (Fig. 5I, J), CCL5 increased, but there was no significant detection of CCL2. This suggests that part of the immune infiltration could be driven by tumor cell-intrinsic cytokine production. Almost without exception, radiation-induced cytokine and chemokine secretion from tumor cells was potentiated by the addition of ATRi.

Discussion

Radiotherapy is a standard of care in many tumor types. It is now well understood that radiotherapy can trigger immune responses and potentially lead to anti-tumor immunity (1). Despite advances in targeted delivery of radiotherapy, normal tissue toxicity imposes a limit upon further dose escalation. Small molecule radiosensitizers such as ATRi present a potential means to improve responses to radiotherapy by increasing tumor-selective cell kill. Through broad profiling of the immune landscape, we have demonstrated preclinical evidence that combination therapy with ATR inhibition can modulate the radiation-induced inflammatory tumor microenvironment.

It has been recognised for some time that radiation has various effects on the tumor microenvironment, in particular the infiltrating immune compartment. These effects can have positive and negative implications for tumor control (1). Radiation is also known to enhance the infiltration of immune suppressive cells, such as $T_{regs,}$ TAMs and MDSCs. These cells may increase the resistance of tumors to therapy and confer pro-malignant properties (4). Available preclinical data suggest there is no increased normal tissue toxicity from the combination of ATRi-RT (22, 23), but little is known about the effect of radiation sensitising drugs on the tumor microenvironment. It is increasingly recognised that targeted therapies may have immunomodulatory effects. For example, CDK4/6 inhibition has been shown to promote anti-tumor immunity, by increasing levels of intracellular double-stranded RNA, stimulating interferon production and antigen presentation, as well as by inhibiting T_{reg} proliferation (24). Treatment of tumor cell lines with PARP inhibitors causes upregulation of PD-L1, through a mechanism involving inactivation of GSK3α/β (25). It is also recognised that modulation of anti-tumor immunity may enhance radiation responses by overcoming the radiation-induced upregulation of immunosuppressive factors. For example, blocking the PD-L1 receptor overcomes radiation resistance, in a CD8-dependent manner (26). The picture that we have observed in this preclinical model is that ATRi in combination with radiation enhances infiltration of almost all immune populations. This appears to be a non-selective amplification of radiation-induced effects. As such, this results in increased infiltration of therapeutically beneficial cells such as dendritic cells and CD8+ CTLs, but also enhancement of potentially suppressive populations.

During the preparation of this manuscript, work by Vendetti and colleagues (27) demonstrated potentiation of radiation-induced cytotoxic T-cell activity when ATRi was added to 2 x 2 Gy radiation, as well as a reversal of the radiation-induced PD-L1 expression on tumor cells, a reduction in tumor-infiltrating T_{regs} and enhanced anti-tumor immunologic

memory in a mouse model of colorectal cancer. Although no comment was made in that work about myeloid populations, the modulation of immune responses by ATRi-RT is notable, and highlights the differences in immune infiltrates and responses to therapy between tumour models, reflecting those seen in patients. This may be due to the differences in immunogenicity of the tumor model used, as well as differences in the capacity to respond to intracytoplasmic nucleic acids the spectrum of cytokines released by the tumour cells in response to DNA damage. We also note that the time point chosen for analysis may result in significant differences in the observed immune infiltrate, as noted by that work.

Functional assays are required to determine if the cd11b+ Gr1+ cells are a truly immunosuppressive cell population, such as MDSCs. MDSCs suppress T-cell functions through depletion of arginine by arginases 1 and 2, and signalling to T-cells which results in dysfunction, proliferative arrest and induction of the T_{reg} phenotype (28). Monocytic MDSC can differentiate into tumor-associated macrophages and inflammatory DCs (29). The functions of macrophages may be immunostimulatory (M1-like) or immunosuppressive (M2-like), depending upon their subtype (30). We have described ATRi amplification of radiation effects as indiscriminate, and this appears to extend to the vast majority of populations investigated. On preliminary analysis, there was no shift in macrophage polarity based on the M2 marker CD206, but further analyses would be required to determine the properties of the infiltrating macrophages. Immunosuppressive DCs have also been described in tumors, expressing indoleamine 2, 3-dioxygenase 1 (IDO-1) which suppresses T-cell activity (31). No significant changes in *Ido1* gene expression were observed in this experiment (but this was not verified on protein level (data not shown)). Little change in subtype proportion was observed for Ly6C and Ly6G subpopulations with CD11b+ Gr-1+ cells.

We were interested in trying to identify the root cause behind the ability of ATRi to enhance radiation-induced immune cell infiltration. Interactions between the DDR and anti-tumor immunity are becoming better understood (6). We have previously shown that the mechanism of radiosensitization by AZD6738 involves mitotic catastrophe with the generation of acentric micronuclei (32). Recent data have shown these micronuclei are subject to breakdown of the micronuclear envelope results in activation of cyclic GMP-AMP synthase (cGAS), which generates cyclic GMP-AMP (cGAMP), activating a type I interferon response via the STING (stimulator of interferon genes) pathway (18). Mitotic progression in the presence of micronuclei is required for their stimulation of immune responses (8). A previous study indicated that DDR-deficient breast tumors were defined by interferon signalling (7). In that study CXCL10 and CCL5 were significantly upregulated in DNA repair

deficient cells in a cGAS/STING dependent manner with chemoattraction of PBMCs dependent on CXCL10 and CCL5. The similarity of radiation and ATRi (a pharmacologically induced DDR defect) in regards to CXCL10 and CCL5 expression was striking.

These recent findings in the literature lead us to look at transcriptional levels of STING where no increase was observed. This does not preclude STING functional activity at a steady gene expression state. Levels of cGAS and transcriptional levels of a number of other potential nucleic acid-sensing proteins were, however, upregulated coinciding with increased *Irf7*. There was a significant increase in Z-DNA-binding protein 1 (*Zbp1*), in ATRi-RT vs. control. ZBP1 is a cytosolic DNA sensor which stimulates type-I interferon production and the production of CXCL10, signalling through IRF3 and IRF7 (20). Cytosolic DNA can also activate RIG-I (*Ddx58*) via DNA-dependent RNA polymerase III signalling (33). RIG-I stimulation has been shown to cause CXCL10 and CCL5 release from tumor cells and upregulate HLA class I (34). Another RNA sensor, interferon-induced helicase C domain-containing protein-1 (*Ifih1*) also causes CXCL10 release upon stimulation (35). Rsad2/viperin was increased under all treatments and is an interferon-inducible gene promoting TLR9 signalling in pDC (15). This pathway detects viral and self-DNA, stimulating the transcription of type 1 interferon by signalling through IRF7. We recognize that other pathways may also be involved in the inflammatory response to radiation, including absent in melanoma 2 (AIM2)(36), whether these are modulated by the addition of ATRi is currently not known.

Due to the 5-day post-radiation timepoint, only indirect evidence of a type-I interferon response after ATRi-RT treatment was shown by the upregulation of multiple interferon-stimulated genes (ISGs) in tumor cells (37). The outlined nucleic acid sensors are known to be ISGs. Hence, we cannot definitively state whether these genes are induced in response to cytosolic nucleic acids directly, or in response to type-I interferon production from a different source. It is unlikely that elevated levels of these proteins are not functionally active in some capacity in sensing cytoplasmic dsDNA in response to radiation and ATRi. Future work is needed to establish the exact functional relevance of these proteins.

In vitro cell line experiments, and gene expression analysis of sorted immune and non-immune cells, showed cytokines produced by proliferating tumor cells subjected to radiation and ATRi are likely to contribute significantly to the immune infiltration observed. In our model, tumor cells alone secreted CXCL10 and CCL5 with combination treatment. CCL5 is chemotactic for macrophages and T-cells, and plays a role in activating NK cells (in conjunction with signals from activated T-cells). Hence, DNA damage may activate DNA-

sensing pathways within the cell to cause release of CXCL10 and CCL5, attracting innate immune cells into the tumor which subsequently activate an adaptive response. CCL5 (i) is a target of NF-κB activity, again released by multiple cell types including immune, stromal and tumor cells, (ii) recruits cells including T-cells and macrophages, and (iii) stimulates NK cell activation. CCL5, along with CCL2, has also been implicated in cancer progression and metastasis, through multiple mechanisms, including the generation of MDSCs (38, 39) (40), and the attraction of inflammatory monocytes which subsequently differentiate into macrophages capable of promoting metastasis (41, 42). CCL2 is secreted by multiple cell types, including tumor cells and endothelial cells, with the major source being monocytes/macrophages (43) Tumor-associated macrophages also produce CCL22 which attracts T_{regs} (31). *Ccl22* is one of the significantly upregulated genes with the ATRi-RT combination vs. control (Fig. 5A, B). Overall, our data support the hypothesis that DNA damage within the tumour cells leads to an interferon response, and cytokine release leading to modulation of the immune microenvironment. The addition of ATRi boosts this radiation induced response.

Publications in the literature have shown positive preclinical results for radiation in combination with anti-PD1 (44) and anti-CTLA4 (45) therapies. Our data point to a myeloid-heavy infiltrate in response to ATRi-RT. This may offer an alternative immuno-oncology angle of attack where anti-PD1 or -CTLA4 fails. Translational research from the ongoing AZD6738 and radiation clinical trial (46) may also give further information about the immunogenicity of the combination. We have chosen to investigate the effects of ATRi on a clinically-relevant radiation dose schedule of 2 Gy per fraction, most commonly used in radical treatments, and the dose per fraction currently being assessed in the clinical study of AZD6738 with radiation (47). We acknowledge that optimal dose-fractionations for immune stimulation are still under investigation, and are likely to be moderately large doses per fraction. The effect of radiosensitizers on these dose-fractionations is the subject of ongoing study, but in the clinic, drug sensitisation of large fractions is avoided due to concerns regarding toxicity. In the radiation field, analysis of fractionation effects with radiosensitizing drugs to see whether they can be optimised not only for tumor kill, but potentially selection of a more favourable profile of immune infiltrates would be of great interest.

In conclusion, we have shown an immunomodulatory effect of ATR inhibition with radiotherapy on the tumor microenvironment. Radiosensitization by ATRi is well established, but to fully exploit the potential of G2/M cell cycle checkpoint-targeted agents in cancer treatment we need to understand the effect of these agents on immune responses. ATR inhibition can boost the immunogenic response to radiotherapy. Understanding the

suppressive immune populations in this context is critical to enhancing anti-tumor immunity in addition to the enhanced tumor control possible through the combination of ATRi and radiation.

References

1. Weichselbaum RR, Liang H, Deng L, Fu YX. Radiotherapy and immunotherapy: a beneficial liaison? Nature reviews Clinical oncology. 2017;14:365-79.
2. Barker HE, Paget JT, Khan AA, Harrington KJ. The tumour microenvironment after radiotherapy: mechanisms of resistance and recurrence. Nature reviews Cancer. 2015;15:409-25.
3. Demaria S, Golden EB, Formenti SC. Role of Local Radiation Therapy in Cancer Immunotherapy. JAMA Oncol. 2015;1:1325-32.
4. Vatner RE, Formenti SC. Myeloid-derived cells in tumors: effects of radiation. Seminars in radiation oncology. 2015;25:18-27.
5. Barber GN. STING: infection, inflammation and cancer. Nat Rev Immunol. 2015;15:760-70.
6. Mouw KW, Goldberg MS, Konstantinopoulos PA, D'Andrea AD. DNA Damage and Repair Biomarkers of Immunotherapy Response. Cancer discovery. 2017;7:675-93.
7. Parkes EE, Walker SM, Taggart LE, McCabe N, Knight LA, Wilkinson R, et al. Activation of STING-Dependent Innate Immune Signaling By S-Phase-Specific DNA Damage in Breast Cancer. Journal of the National Cancer Institute. 2017;109.
8. Harding SM, Benci JL, Irianto J, Discher DE, Minn AJ, Greenberg RA. Mitotic progression following DNA damage enables pattern recognition within micronuclei. Nature. 2017;548:466-70.
9. Vanneman M, Dranoff G. Combining Immunotherapy and Targeted Therapies in Cancer Treatment. Nature reviews Cancer. 2012;12:237-51.
10. Workman P, Aboagye EO, Balkwill F, Balmain A, Bruder G, Chaplin DJ, et al. Guidelines for the welfare and use of animals in cancer research. British journal of cancer. 2010;102:1555-77.
11. Lin KY, Guarnieri FG, Staveley-O'Carroll KF, Levitsky HI, August JT, Pardoll DM, et al. Treatment of established tumors with a novel vaccine that enhances major histocompatibility class II presentation of tumor antigen. Cancer research. 1996;56:21-6.
12. Dillon MT, Espinasse A, Ellis S, Mohammed K, Grove LG, McLellan L, et al. Abstract CT084: A Phase I dose-escalation study of ATR inhibitor monotherapy with AZD6738 in advanced solid tumors (PATRIOT Part A). Cancer research. 2017;77:CT084-CT.
13. Samarajiwa SA, Forster S, Auchettl K, Hertzog PJ. INTERFEROME: the database of interferon regulated genes. Nucleic acids research. 2009;37:D852-D7.
14. Marvel D, Gabrilovich DI. Myeloid-derived suppressor cells in the tumor microenvironment: expect the unexpected. The Journal of clinical investigation. 2015;125:3356-64.
15. Swiecki M, Colonna M. The multifaceted biology of plasmacytoid dendritic cells. Nat Rev Immunol. 2015;15:471-85.
16. Kuang DM, Zhao Q, Peng C, Xu J, Zhang JP, Wu C, et al. Activated monocytes in peritumoral stroma of hepatocellular carcinoma foster immune privilege and disease progression through PD-L1. The Journal of experimental medicine. 2009;206:1327-37.
17. Lu C, Redd PS, Lee JR, Savage N, Liu K. The expression profiles and regulation of PD-L1 in tumor-induced myeloid-derived suppressor cells. Oncoimmunology. 2016;5:e1247135.

18. Mackenzie KJ, Carroll P, Martin CA, Murina O, Fluteau A, Simpson DJ, et al. cGAS surveillance of micronuclei links genome instability to innate immunity. Nature. 2017;548:461-5.
19. Paludan SR, Bowie AG. Immune sensing of DNA. Immunity. 2013;38:870-80.
20. Takaoka A, Wang Z, Choi MK, Yanai H, Negishi H, Ban T, et al. DAI (DLM-1/ZBP1) is a cytosolic DNA sensor and an activator of innate immune response. Nature. 2007;448:501-5.
21. Miyashita M, Oshiumi H, Matsumoto M, Seya T. DDX60, a DEXD/H box helicase, is a novel antiviral factor promoting RIG-I-like receptor-mediated signaling. Molecular and cellular biology. 2011;31:3802-19.
22. Dunne V, Ghita M, Small DM, Coffey CBM, Weldon S, Taggart CC, et al. Inhibition of ataxia telangiectasia related-3 (ATR) improves therapeutic index in preclinical models of non-small cell lung cancer (NSCLC) radiotherapy. Radiotherapy and Oncology. 2017;124:475-81.
23. Vendetti FP, Leibowitz BJ, Barnes J, Schamus S, Kiesel BF, Abberbock S, et al. Pharmacologic ATM but not ATR kinase inhibition abrogates p21-dependent G1 arrest and promotes gastrointestinal syndrome after total body irradiation. Scientific Reports. 2017;7:41892.
24. Goel S, DeCristo MJ, Watt AC, BrinJones H, Sceneay J, Li BB, et al. CDK4/6 inhibition triggers anti-tumour immunity. Nature. 2017;548:471-5.
25. Jiao S, Xia W, Yamaguchi H, Wei Y, Chen MK, Hsu JM, et al. PARP Inhibitor Upregulates PD-L1 Expression and Enhances Cancer-Associated Immunosuppression. Clinical cancer research : an official journal of the American Association for Cancer Research. 2017;23:3711-20.
26. Dovedi SJ, Adlard AL, Lipowska-Bhalla G, McKenna C, Jones S, Cheadle EJ, et al. Acquired resistance to fractionated radiotherapy can be overcome by concurrent PD-L1 blockade. Cancer research. 2014;74:5458-68.
27. Vendetti FP, Karukonda P, Clump DA, Teo T, Lalonde R, Nugent K, et al. ATR kinase inhibitor AZD6738 potentiates CD8+ T cell-dependent antitumor activity following radiation. The Journal of clinical investigation. 2018;128:3926-40.
28. Marigo I, Dolcetti L, Serafini P, Zanovello P, Bronte V. Tumor-induced tolerance and immune suppression by myeloid derived suppressor cells. Immunol Rev. 2008;222:162-79.
29. Veglia F, Perego M, Gabrilovich D. Myeloid-derived suppressor cells coming of age. Nat Immunol. 2018;19:108-19.
30. Szebeni GJ, Vizler C, Nagy LI, Kitajka K, Puskas LG. Pro-Tumoral Inflammatory Myeloid Cells as Emerging Therapeutic Targets. International journal of molecular sciences. 2016;17:1958.
31. Gabrilovich DI, Ostrand-Rosenberg S, Bronte V. Coordinated regulation of myeloid cells by tumours. Nat Rev Immunol. 2012;12:253-68.
32. Dillon MT, Barker HE, Pedersen M, Hafsi H, Bhide SA, Newbold KL, et al. Radiosensitization by the ATR Inhibitor AZD6738 through Generation of Acentric Micronuclei. Molecular cancer therapeutics. 2017;16:25-34.
33. Chiu Y-H, MacMillan JB, Chen ZJ. RNA Polymerase III Detects Cytosolic DNA and Induces Type I Interferons through the RIG-I Pathway. Cell. 2009;138:576-91.
34. Kubler K, Gehrke N, Riemann S, Bohnert V, Zillinger T, Hartmann E, et al. Targeted activation of RNA helicase retinoic acid-inducible gene-I induces proimmunogenic apoptosis of human ovarian cancer cells. Cancer research. 2010;70:5293-304.
35. Glas M, Coch C, Trageser D, Dassler J, Simon M, Koch P, et al. Targeting the cytosolic innate immune receptors RIG-I and MDA5 effectively counteracts cancer cell heterogeneity in glioblastoma. Stem Cells. 2013;31:1064-74.
36. Hu B, Jin C, Li HB, Tong J, Ouyang X, Cetinbas NM, et al. The DNA-sensing AIM2 inflammasome controls radiation-induced cell death and tissue injury. Science. 2016;354:765-8.
37. Schneider WM, Chevillotte MD, Rice CM. Interferon-stimulated genes: a complex web of host defenses. Annu Rev Immunol. 2014;32:513-45.

38. Aldinucci D, Colombatti A. The Inflammatory Chemokine CCL5 and Cancer Progression. Mediators of Inflammation. 2014;2014:292376.
39. Zhang Y, Lv D, Kim H-J, Kurt RA, Bu W, Li Y, et al. A novel role of hematopoietic CCL5 in promoting triple-negative mammary tumor progression by regulating generation of myeloid-derived suppressor cells. Cell Research. 2013;23:394-408.
40. Kumar V, Patel S, Tcyganov E, Gabrilovich DI. The Nature of Myeloid-Derived Suppressor Cells in the Tumor Microenvironment. Trends Immunol. 2016;37:208-20.
41. Qian B-Z, Li J, Zhang H, Kitamura T, Zhang J, Campion LR, et al. CCL2 recruits inflammatory monocytes to facilitate breast tumor metastasis. Nature. 2011;475:222-5.
42. Lim SY, Yuzhalin AE, Gordon-Weeks AN, Muschel RJ. Targeting the CCL2-CCR2 signaling axis in cancer metastasis. Oncotarget. 2016;7:28697-710.
43. Deshmane SL, Kremlev S, Amini S, Sawaya BE. Monocyte Chemoattractant Protein-1 (MCP-1): An Overview. Journal of Interferon & Cytokine Research. 2009;29:313-26.
44. Oweida A, Lennon S, Calame D, Korpela S, Bhatia S, Sharma J, et al. Ionizing radiation sensitizes tumors to PD-L1 immune checkpoint blockade in orthotopic murine head and neck squamous cell carcinoma. Oncoimmunology. 2017;6:e1356153.
45. Dewan MZ, Galloway AE, Kawashima N, Dewyngaert JK, Babb JS, Formenti SC, et al. Fractionated but not single-dose radiotherapy induces an immune-mediated abscopal effect when combined with anti-CTLA-4 antibody. Clinical cancer research : an official journal of the American Association for Cancer Research. 2009;15:5379-88.
46. Dillon M, Ellis S, Grove L, McLellan L, Clack G, Smith DS, et al. PATRIOT: A phase I study to assess the tolerability, safety and biological effects of a specific ataxia telangiectasia and Rad3-related (ATR) inhibitor (AZD6738) as a single agent and in combination with palliative radiation therapy in patients with solid tumours. ASCO Meeting Abstracts. 2016;34:TPS2603.
47. Dillon MT, Boylan Z, Smith D, Guevara J, Mohammed K, Peckitt C, et al. PATRIOT: A phase I study to assess the tolerability, safety and biological effects of a specific ataxia telangiectasia and Rad3-related (ATR) inhibitor (AZD6738) as a single agent and in combination with palliative radiation therapy in patients with solid tumours. Clin Transl Radiat Oncol. 2018;12:16-20.

Figure Legends

Figure 1: AZD678 therapeutic efficacy combined with fractionated radiotherapy in vivo corresponds to increased CD3+ and B220+ cell infiltration by IHC.
A, Relative tumor growth curves for C57Bl/6 mice carrying subcutaneous TC1 tumors, treated with vehicle, AZD6738 75 mg/kg daily for 5 days, radiation 2 Gy x 4 (daily fractions), or AZD6738 with radiation; the first dose of AZD6738 was administered 2 h prior to irradiation and the last dose was administered the day after the final fraction of radiation. Asterisk represents $p < 0.05$ between radiation and radiation + ATRi curves by unpaired t-test. Minimum 10 animals per group. **B**, quantification of TC1 tumors from (A) stained for CD3 by immunohistochemistry. Minimum 10 fields of view and at least 3 tumors analysed per condition. Average number per field is shown for each tumor, tumors were harvested 5 days after the last fraction of radiation was administered. **C**, quantification of B220-positive cells, as per (B).

Figure 2: Nanostring gene expression analysis reveals AZD6738 significantly modules radiation induced immune-linked transcripts in vivo.
A, Overview of differential gene expression with ATR-radiation combinations in the TC-1 murine model at 5 days after the end of 4 x 2 Gy radiation in the presence or absence of AZD6738. Differential expression analysis of NanoString data was performed, and gene functional annotations used to classify each gene with significantly altered expression into one of the above groups. Genes with significant change in expression (with $p < 0.05$ by Benjamini-Yekutieli Method) were grouped into functional categories and the number of genes with significant differential expression per category is shown for the indicated pairwise comparisons. Legend indicates which two groups were compared.
B, Venn diagram illustrating numbers of genes with significant changes in expression for the indicated combinations. C, Venn diagram illustrating interferon-stimulated genes, for ATRi-RT combination treatment. The number of genes stimulated by each of type I, II and III interferons is demonstrated. Overall, there is a greater representation of genes that are stimulated by type I interferons in the database, and very few by type III interferons, so this may lead to a degree of bias in these results (from Interferome database).

Figure 3: AZD6738 increases radiation induced lymphoid infiltration in vivo.
A, number of lymphoid cells per mg tumor was calculated 5 days after the end of 4 x 2 Gy radiation in the presence or absence of AZD6738. Error bars: SD (one direction only if lower SD outside the plotted area), asterisks: statistical significance by ANOVA with multiple comparisons, Min. 3 independent repeats of at least 3 animals per group. Populations were identified by the markers: CD3, CD3+; CD4eff, CD3+CD4+FOXP3-; T_{reg}, CD3+CD4+FOXP3+; CD8, CD3+CD8+; NK, CD3-B220-NK1.1+; B cell, B220+. **B**, change in proportion of Granzyme B (GzB+) or Ki67+ CD8+ cells as a proportion of total CD8+ cells, and Ki67+ (proliferating) cells as a proportion of total CD4+FOXP3- or CD4+FOXP3+ cells. Error bars: SEM. **C**, mRNA transcript fold change in whole tumor lysates at 5 days after completion of radiotherapy. Copy number normalised to median controls. Mean and SD plotted, asterisks: statistical significance by ANOVA with multiple comparisons. **D**, change in proportion of effector, regulatory and CD8-positive T cells, as a function of total CD3-positive cells, and Ki67-positive T_{reg}, T_{eff} and CD8 positive, as a proportion of total T_{reg}, T_{eff} and CD8-positive cells, in draining lymph node (ipsilateral inguinal node), five days after completion of radiotherapy, min. 3 animals per group. **E**, normalised fluorescence intensity (normalised to mean of control fluorescence) of effector CD4 T-cells (CD3+, CD4+, FoxP3-), for the indicated markers of activation in tumor infiltrating cells in TC-1 tumors 5 days after the end of 4 x 2 Gy radiation in the presence or absence of AZD6738. Minimum 3 animals per group

in 2 independent experiments. F, fold-change mRNA transcript counts for corresponding genes indicating T cell activation, in a cell population sorted for CD45 in ATRi-RT treated tumours, relative to the median value for the control samples of each gene, mean and SD are plotted, asterisks: significance by unpaired t-test between ATRi-RT and control

Figure 4, AZD6738 increases radiation induced myeloid infiltration *in vivo*.
A, Assessment of tumor infiltrating myeloid cells at day 5 after treatment. Populations were identified as follows: B cells, B220+; dendritic cells, CD11c+ MHCII+; macrophages (Mac), CD11b+ CD11c- CD68+ SSC^{Low}, MHC-2+, Gr-$1^{Low-Int}$; CD11b+ Gr-1^{Int-Hi} NK1.1- CD3-. Asterisks: statistical significance by ANOVA with multiple comparisons testing. **B**, Proportions of CD206-positive and negative tumor-infiltrating macrophages, as a marker of M2a and M2c macrophages. **C**, proportions of CD11b+Gr-1+ subsets: proportions of CD11b+ $Ly6C^{High}$ for monocytic and $Ly6C^{Low}$ for granulocytic, no significant difference between control and ATRi+RT; **D**, Dendritic cells (CD11C+ MHC2+) were stained with B220, a marker of plasmacytoid DC. Proportion of parent shown. **E**, Flow cytometric analysis of PD-L1 staining for the indicated tumor subpopulations: CK+ indicates pan-cytokeratin positive cells, a surrogate for tumor cells. Mac = Macrophages (CD11b+, CD3-, NK1.1-, $CD11c^{Low}$, CD68+, MHCII+, $Gr1^{Low-int}$); Gr-1 = CD11b+, Gr1+, CD3- NK1.1-. **F**, mRNA counts for PD-L1 (*Cd274*), expressed as fold change in ATRi-RT treated tumours compared with control, in tumour populations sorted by CD45 status. **G**, flow cytometric analysis of tumor cells (pan-cytokeratin positive), showing mean fluorescence intensity for MHC-1 (mouse: H-2Kb). Mean fluorescence normalised to average control value. **H**, mRNA expression of genes involved in antigen processing and presentation, fold change in ATRi-RT vs. control, expressed as fold change in ATRi-RT treated tumours compared with control, in tumour populations sorted by CD45 status. All panels: 5 days after the end of treatment with 4 x 2 Gy radiation in the presence or absence of AZD6738. Minimum 3 tumors per condition, 2 independent experiments. significance: ANOVA with multiple comparisons (except F, H: unpaired t-test), mean and SD displayed.

Figure 5, ATRi-RT causes modulation of cytokine production
Analysis of changes in cytokine expression with ATR—radiation combinations, 5 days after treatment with 4 x 2 Gy radiation in the presence or absence of AZD6738. **A**, mRNA expression data, only statistically significant changes are displayed. Mean of 3 replicates displayed. Fold change from control tumors displayed. Grey boxes: no significant difference found. **B**, Cytokine, chemokine, and receptor transcript analysis, as for (A), in tumour populations sorted by CD45-status. Grey boxes: no transcripts. **C,** protein expression by cytokine array. Densitometry of array was measured and then normalised to positive and negative controls. Two tumors per group were analysed in duplicate. Mean of 2, Log_2 fold change replicates displayed. **D**, western blot showing changes in the indicated proteins in *in vivo* samples after vehicle or ATRi+RT treatment, 5 days after the end of irradiation. **E**, mRNA expression of toll-like receptor (TLR) transcripts. **F,** mRNA expression of interferon regulatory factor (IRF) transcripts. **G,** mRNA expression of the indicated nucleic acid-sensing proteins. A-G: at 5 days after the final dose of radiotherapy, 3 animals per group, mean and S.D. displayed, analysed by ANOVA with multiple comparisons. **H,** Analysis of transcripts for nucleic acid sensors as for (G), on sorted populations of CD45-positive and –negative tumour cells. Asterisk: significance by unpaired t-test compared with control group for same cell population. **I, J,** measurement of cytokine concentration in supernatant of tumor cell lines FaDu (I) and HN5 (J) at 72 hours after treatment with DMSO, AZD6738 (0.5 μM), an 8 Gy fraction of radiation, or radiation in combination with AZD6738 (added 1 hour prior to irradiation). Supernatant was analysed by mutliplex bead-based flow cytometry. Only analytes detected above lower limit of quantification are displayed. Mean of two independent experiments, each run in duplicate, displayed.

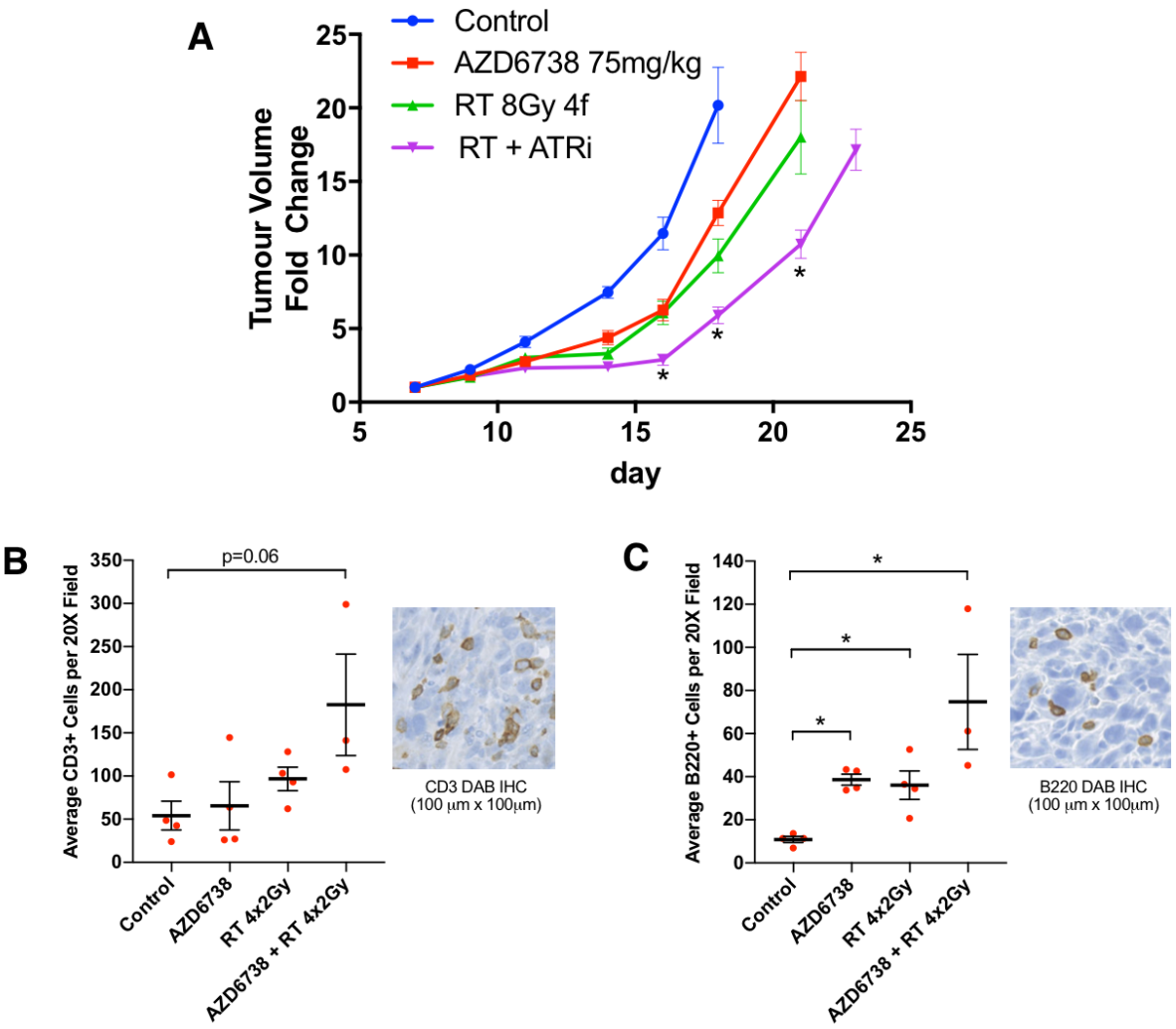
A
Control
AZD6738 75mg/kg
RT 8Gy 4f
RT + ATRi
Tumour Volume
Fold Change
day
B
p=0.06
Average CD3+ Cells per 20X Field
Control
AZD6738
RT 4x2Gy
AZD6738 + RT 4x2Gy
CD3 DAB IHC
(100 μm x 100μm)
C
Average B220+ Cells per 20X Field
Control
AZD6738
RT 4x2Gy
AZD6738 + RT 4x2Gy
B220 DAB IHC
(100 μm x 100μm)

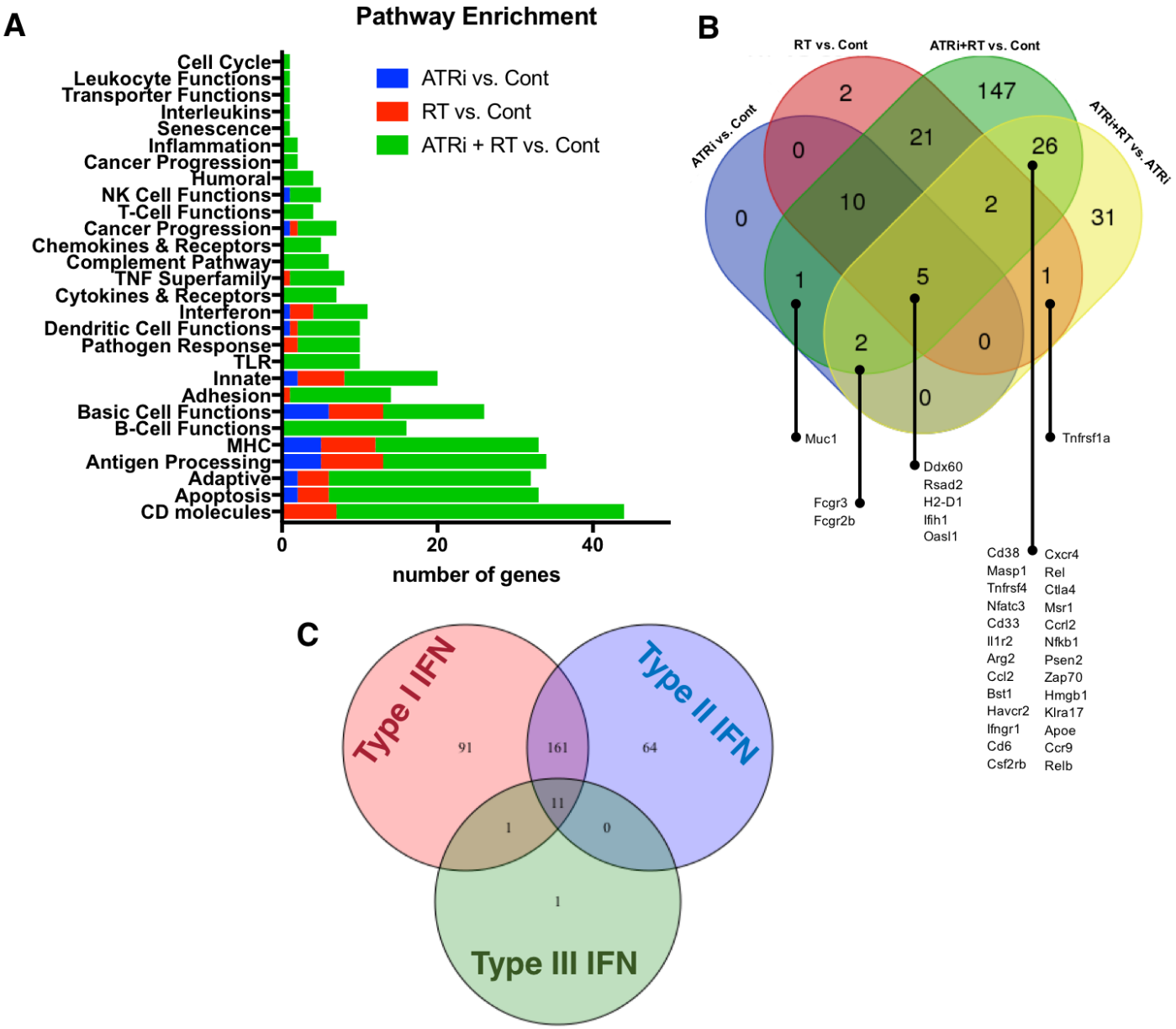
A
Pathway Enrichment
ATRi vs. Cont
RT vs. Cont
ATRi + RT vs. Cont
Cell Cycle
Leukocyte Functions
Transporter Functions
Interleukins
Senescence
Inflammation
Cancer Progression
Humoral
NK Cell Functions
T-Cell Functions
Cancer Progression
Chemokines & Receptors
Complement Pathway
TNF Superfamily
Cytokines & Receptors
Interferon
Dendritic Cell Functions
Pathogen Response
TLR
Innate
Adhesion
Basic Cell Functions
B-Cell Functions
MHC
Antigen Processing
Adaptive
Apoptosis
CD molecules
0
20
40
number of genes
B
RT vs. Cont
ATRi+RT vs. Cont
ATRi vs. Cont
ATRi+RT vs. ATRi
2
147
0
21
26
0
10
2
31
1
5
1
2
0
0
Muc1
Fcgr3
Fcgr2b
Ddx60
Rsad2
H2-D1
Ifih1
Oasl1
Tnfrsf1a
Cd38
Masp1
Tnfrsf4
Nfatc3
Cd33
Il1r2
Arg2
Ccl2
Bst1
Havcr2
Ifngr1
Cd6
Csf2rb
Cxcr4
Rel
Ctla4
Msr1
Ccrl2
Nfkb1
Psen2
Zap70
Hmgb1
Klra17
Apoe
Ccr9
Relb
C
Type I IFN
Type II IFN
Type III IFN
91
161
64
11
1
0
1

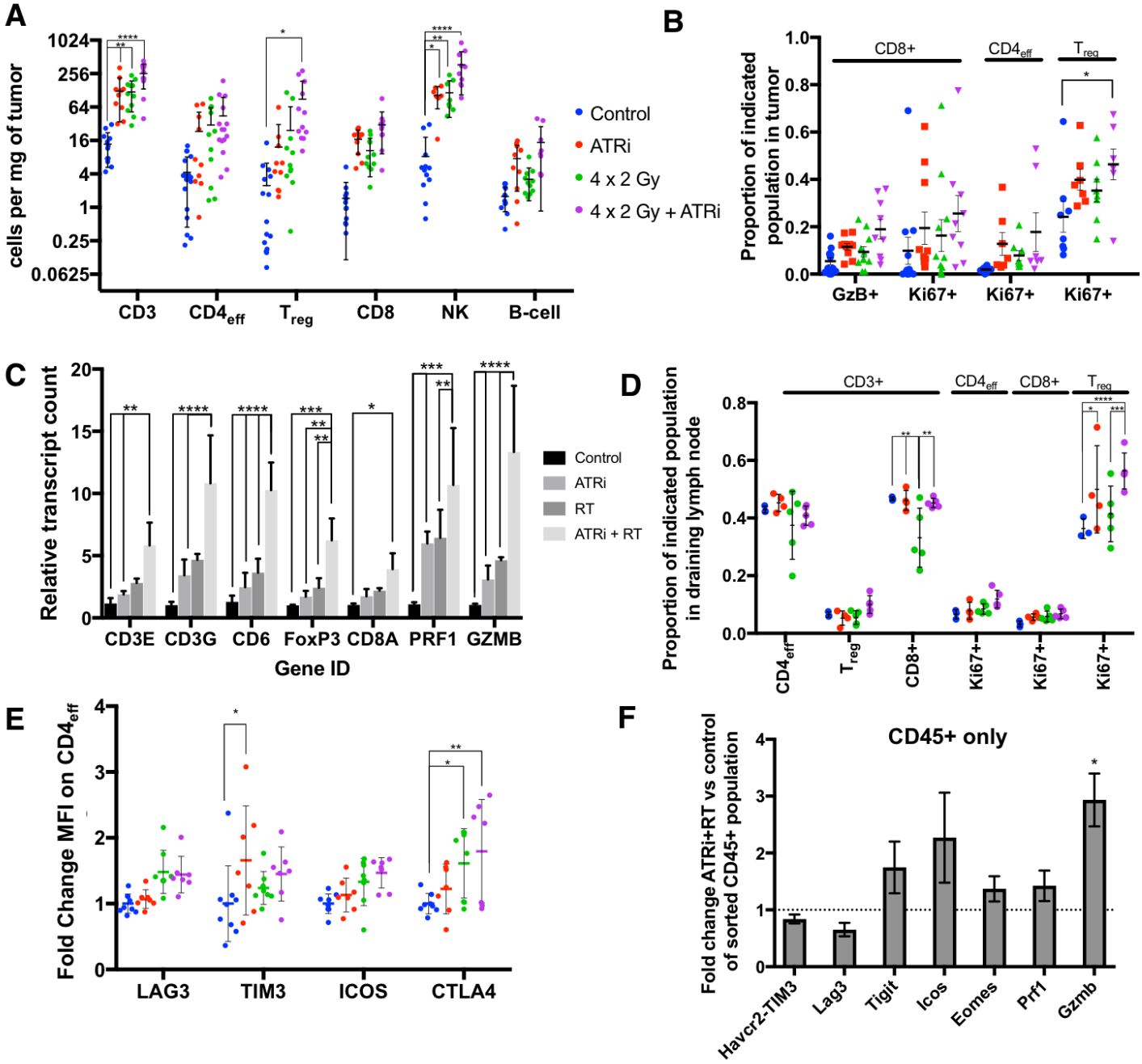
A
cells per mg of tumor
1024
256
64
16
4
1
0.25
0.0625
CD3
CD4eff
Treg
CD8
NK
B-cell
Control
ATRi
4 x 2 Gy
4 x 2 Gy + ATRi
B
Proportion of indicated population in tumor
CD8+
CD4eff
Treg
GzB+
Ki67+
Ki67+
Ki67+
C
Relative transcript count
CD3E
CD3G
CD6
FoxP3
CD8A
PRF1
GZMB
Gene ID
Control
ATRi
RT
ATRi + RT
D
Proportion of indicated population in draining lymph node
CD3+
CD4eff
CD8+
Treg
CD4eff
Treg
CD8+
Ki67+
Ki67+
Ki67+
E
Fold Change MFI on CD4eff
LAG3
TIM3
ICOS
CTLA4
F
CD45+ only
Fold change ATRi+RT vs control of sorted CD45+ population
Havcr2-TIM3
Lag3
Tigit
Icos
Eomes
Prf1
Gzmb

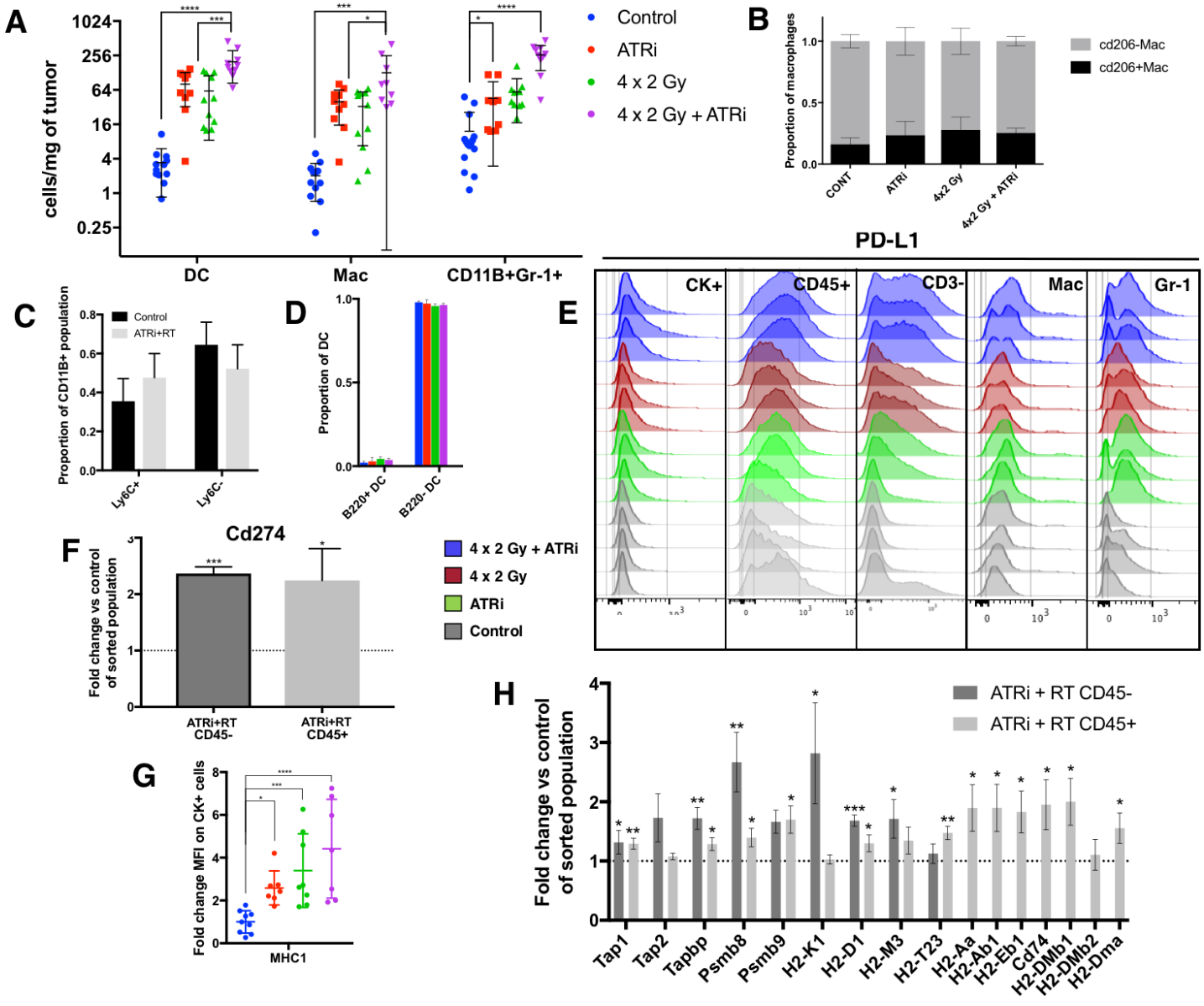
A
cells/mg of tumor
1024
256
64
16
4
1
0.25
DC
Mac
CD11B+Gr-1+
Control
ATRi
4 x 2 Gy
4 x 2 Gy + ATRi
B
Proportion of macrophages
cd206-Mac
cd206+Mac
CONT
ATRi
4x2 Gy
4x2 Gy + ATRi
C
Proportion of CD11B+ population
Control
ATRi+RT
Ly6C+
Ly6C-
D
Proportion of DC
B220+ DC
B220- DC
E
PD-L1
CK+
CD45+
CD3-
Mac
Gr-1
F
Cd274
Fold change vs control of sorted population
ATRi+RT CD45-
ATRi+RT CD45+
4 x 2 Gy + ATRi
4 x 2 Gy
ATRi
Control
G
Fold change MFI on CK+ cells
MHC1
H
Fold change vs control of sorted population
ATRi + RT CD45-
ATRi + RT CD45+
Tap1
Tap2
Tapbp
Psmb8
Psmb9
H2-K1
H2-D1
H2-M3
H2-T23
H2-Aa
H2-Ab1
H2-Eb1
Cd74
H2-DMb1
H2-DMb2
H2-Dma

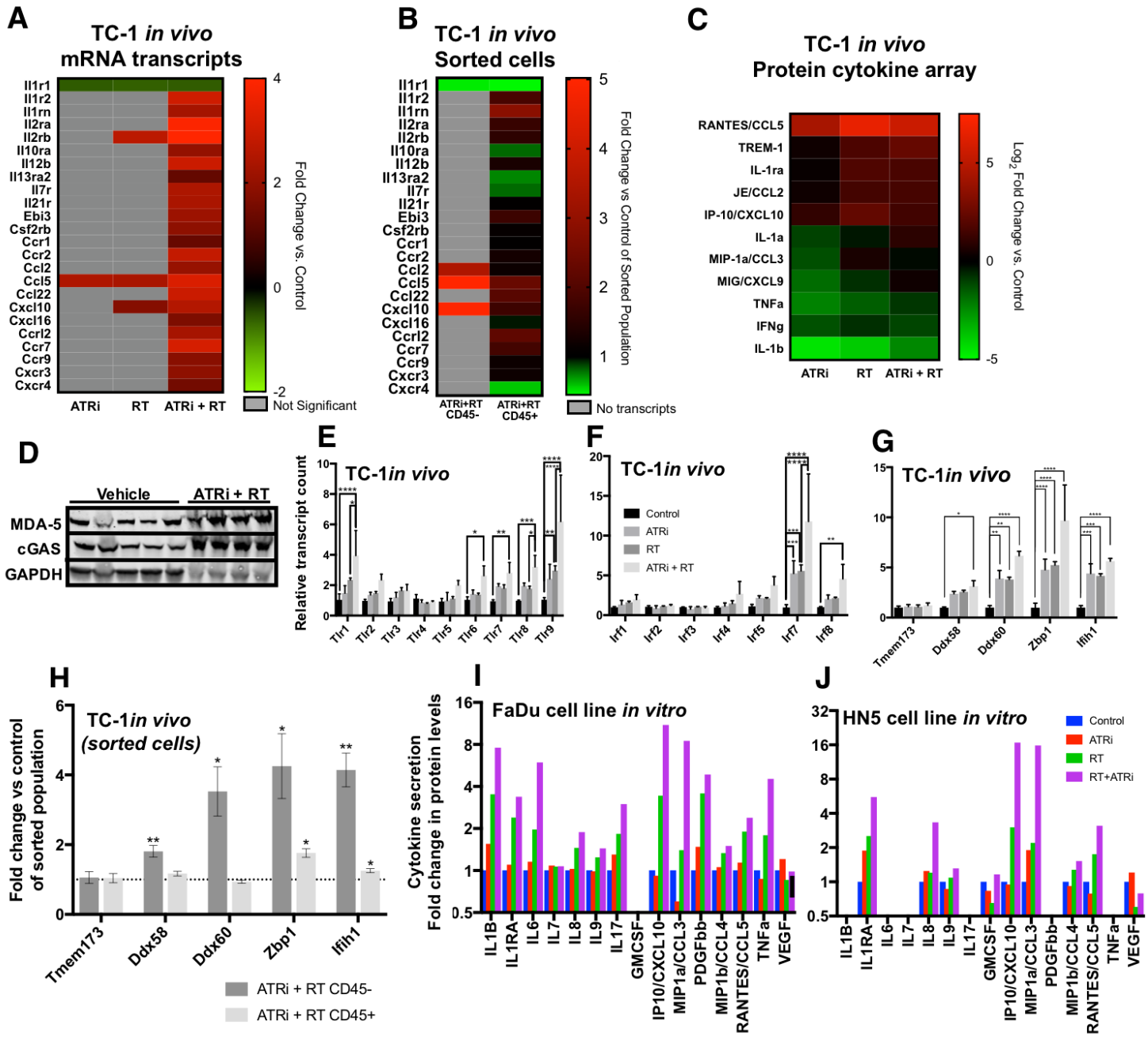
A
TC-1 in vivo
mRNA transcripts
Il1r1
Il1r2
Il1rn
Il2ra
Il2rb
Il10ra
Il12b
Il13ra2
Il7r
Il21r
Ebi3
Csf2rb
Ccr1
Ccr2
Ccl2
Ccl5
Ccl22
Cxcl10
Cxcl16
Ccrl2
Ccr7
Ccr9
Cxcr3
Cxcr4
ATRi
RT
ATRi + RT
4
2
0
-2
Fold Change vs. Control
Not Significant
B
TC-1 in vivo
Sorted cells
ATRi+RT CD45-
ATRi+RT CD45+
5
4
3
2
1
Fold Change vs Control of Sorted Population
No transcripts
C
TC-1 in vivo
Protein cytokine array
RANTES/CCL5
TREM-1
IL-1ra
JE/CCL2
IP-10/CXCL10
IL-1a
MIP-1a/CCL3
MIG/CXCL9
TNFa
IFNg
IL-1b
ATRi
RT
ATRi + RT
5
0
-5
Log2 Fold Change vs. Control
D
Vehicle
ATRi + RT
MDA-5
cGAS
GAPDH
E
TC-1in vivo
Relative transcript count
Tlr1
Tlr2
Tlr3
Tlr4
Tlr5
Tlr6
Tlr7
Tlr8
Tlr9
F
TC-1in vivo
Control
ATRi
RT
ATRi + RT
Irf1
Irf2
Irf3
Irf4
Irf5
Irf7
Irf8
G
TC-1in vivo
Tmem173
Ddx58
Ddx60
Zbp1
Ifih1
H
TC-1in vivo
(sorted cells)
Fold change vs control
of sorted population
Tmem173
Ddx58
Ddx60
Zbp1
Ifih1
ATRi + RT CD45-
ATRi + RT CD45+
I
FaDu cell line in vitro
Cytokine secretion
Fold change in protein levels
IL1B
IL1RA
IL6
IL7
IL8
IL9
IL17
GMCSF
IP10/CXCL10
MIP1a/CCL3
PDGFbb
MIP1b/CCL4
RANTES/CCL5
TNFa
VEGF
J
HN5 cell line in vitro
Control
ATRi
RT
RT+ATRi
IL1B
IL1RA
IL6
IL7
IL8
IL9
IL17
GMCSF
IP10/CXCL10
MIP1a/CCL3
PDGFbb
MIP1b/CCL4
RANTES/CCL5
TNFa
VEGF